Available online at www.sciencedirect.com
ScienceDirect
Icarus 195 (2008) 378–385
ICARUS
www.elsevier.com/locate/icarus

Numerical modeling of endogenic thermal anomalies on Europa

Oleg Abramov *, John R. Spencer

Department of Space Studies, Southwest Research Institute, 1050 Walnut St., Suite 300, Boulder, CO 80302, USA

Received 2 April 2007; revised 11 November 2007

Available online 8 January 2008

Abstract

A variety of recent resurfacing features have been observed on Europa, which may produce thermal anomalies detectable by a future mission. However, the likelihood of such a detection depends on their size and lifetimes. The results of this numerical study suggest that the lifetime of a thermal anomaly associated with the emplacement of 100 m of water onto the surface of Europa is several hundred years, and ∼10 years for 10 m of water. If warm ice is emplaced on the surface instead of liquid water, these lifetimes decrease by up to a factor of two. Exploration of model parameters indicates that a thin insulating surface layer can double thermal anomaly lifetimes, anomalies emplaced at a latitude of 80° can remain detectable nearly a factor of two longer than those at equatorial latitudes, and anomalies on the night side can remain detectable for up to ∼20% longer than those on the day side. High temperatures are very short-lived as the surface ice cools very rapidly to below 200 K due to sublimation cooling. Assuming steady-state resurfacing, the number of detectable thermal anomalies associated with the emplacement of 100 m of water would be on the order of 10 if the typical resurfacing area is 15 km^2. If recent resurfacing is dominated by chaos regions with typical areas of 100 to 1000 km^2 and lifetimes of 1000 to 4000 years, the number of detectable thermal anomalies would be on the order of 1 to 10.

Keywords: Europa; Geological processes; Ices; Thermal histories; Volcanism

1. Introduction and objectives

Jupiter's Galilean satellite Europa is of great scientific interest, largely because of an inferred presence of a ∼100 km deep briny ocean beneath its icy shell, as suggested by surface geology (e.g., Carr et al., 1998; Hoppa et al., 1999; Pappalardo et al., 1999), and strengthened by Galileo magnetometer measurements (e.g., Khurana et al., 1998; Kivelson et al., 2000). Also of great interest is the strong possibility of ongoing endogenic activity, probably driven by tidal effects caused by the Laplace resonance of Europa with Io and Ganymede (Hussmann and Spohn, 2004), which is supported by a young average surface age of ∼60 Ma (Zahnle et al., 1998; Pappalardo et al., 1999; Schenk et al., 2004). This possibility is strengthened by the recent discovery of present-day endogenic thermal anomalies at the south polar regions of Enceladus. A wide variety of resurfacing features have been observed on Europa, including lenticulae, bands, ridges, chaos, and apparent cryovolcanic features, which consist of flooding of portions of Europa's surface (e.g., Pappalardo et al., 1999). Examples of resurfacing styles on Europa are illustrated in Fig. 1.

In addition to the clearly cryovolcanic features, most of the resurfacing features outlined above likely involve delivery of warm material from depth to the near-surface and thus a formation of a thermal anomaly, which may be detectable by a thermal mapping instrument on a future Europa mission. Pits, domes, and dark spots, collectively termed "lenticulae," have been interpreted as diapiric intrusions beneath a relatively thin surface layer or extrusion of warm diapiric material onto the surface (e.g., Pappalardo et al., 1998). Alternatively, it was suggested by Fagents et al. (1998) that some lenticulae form from cryovolcanically extruded slurries. Pull-apart bands were likely formed as a result of movement of the brittle surface layer atop warm, mobile, low-viscosity material in the shallow subsurface (e.g., Pappalardo et al., 1999), possibly exposing warm material in the process. Of the several proposed models that explain ridge formation on Europa—volcanism (Kadel et al., 1998), tidal squeezing (Greenberg et al., 1998), diapirism (Head et al., 1998), compression (Sullivan et al., 1997), and wedging

* Corresponding author. Fax: +1 303 546 9687.
E-mail address: abramovo@boulder.swri.edu (O. Abramov).

0019-1035/$ – see front matter
doi:10.1016/j.icarus.2007.11.027

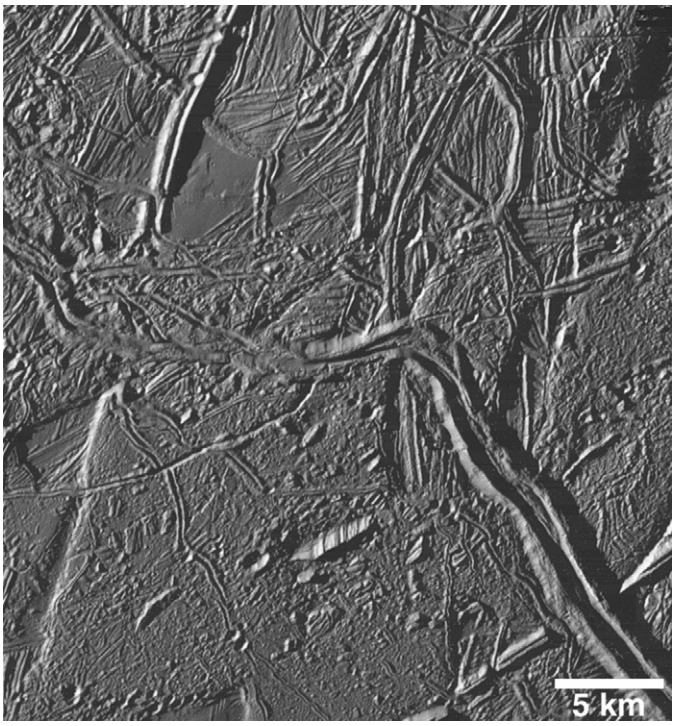

Fig. 1. Examples of resurfacing styles on Europa, from a region near Europa's south pole (80.82° S, 132.99° W), showing doublet ridges, chaos with raised margins (emplacement as warm solid ice?), and smooth plains in a depression (liquid-state emplacement?). Galileo image ID 17E0078.

(Melosh and Turtle, 2004)—all but one (compression) involve delivery of liquid water or warm ice to the surface. Finally, several models for chaos features have been proposed: melt-through of the subsurface ocean (e.g., Greenberg et al., 1999; O'Brien et al., 2002), solid-state convection (Pappalardo et al., 1998; McKinnon, 1999), diapirism (e.g., Sotin et al., 2002), and brine mobilization (Head and Pappalardo, 1999). All of these proposed mechanisms involve delivery of liquid water or warm ice to the surface.

Thermal observations might be the best way to identify areas which are currently geologically active, and are thus likely to have the thinnest crust. These areas would be prime landing spots for a potential lander. However, the likelihood of such a detection depends on the size and lifetimes of endogenic thermal anomalies, which were approximated analytically by Van Cleve et al. (1999) and are modeled numerically in this work.

The simplest form of such an anomaly is a body of warm ice or liquid water emplaced onto the surface, with horizontal extent much larger than its thickness so it can be modeled one dimensionally (Fig. 2). This geometry can be used to describe most resurfacing features outlined above with varying degrees of accuracy. Although this simple model does not explicitly describe all landforms, approximations can nonetheless be used to derive useful estimates. In this work, we model liquid water and warm ice bodies with thicknesses of 1, 10, and 100 m. In addition, a 10-km thick chaos model was constructed. As described above, proposed chaos formation mechanisms involve delivery of liquid water or warm ice to the surface, so both cases have been modeled. Model predictions include diurnal surface

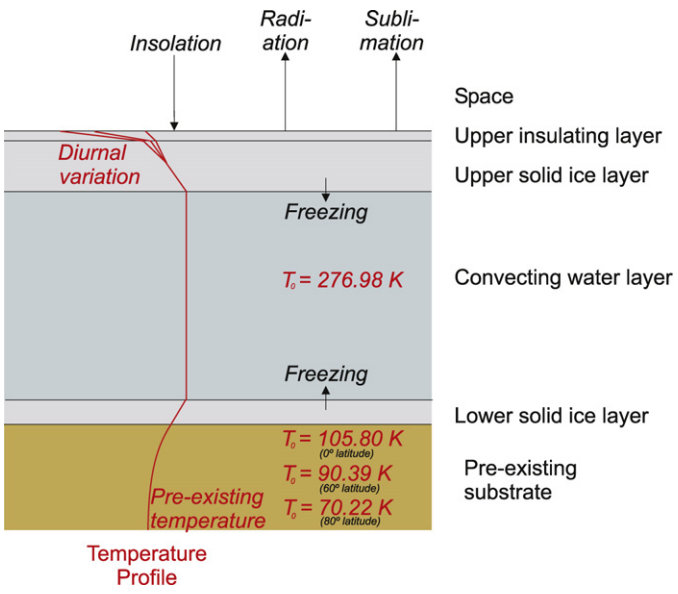

Fig. 2. General schematic of the model.

temperatures in the region of the thermal anomaly, as well as detectable lifetimes as a function of thickness of the water layer.

2. Methodology and techniques

We use an in-house numerical 1-D model (IDL code available from the authors) to track the thermal evolution of liquid water or warm ice bodies emplaced onto the surface of Europa. The model employs a commonly used explicit finite-difference method (e.g., Ketkar, 1999) to calculate transient heat conduction. The model also includes convection (in liquid water), radiation (at the surface), latent heat of fusion, depth and temperature dependent thermophysical parameters, surface absorption of sunlight, rotational modulation of insolation, and cooling by sublimation of surface ice. The overall model setup is shown in Fig. 2.

The only heat sources in our models are the endogenic thermal anomaly and solar insolation. Although tidal heating and radiogenic heating are likely important in keeping the ocean in a liquid state, they are less significant in the upper cryosphere, which is modeled in this paper. Tidal heating is concentrated at the base of the cryosphere where, because of its strong temperature-dependent viscosity, the ice is more dissipative at the timescale of tidal flexing (3.55 days) (Ojakangas and Stevenson, 1989); and radiogenic heating is concentrated in the silicate interior (e.g., Sotin and Tobie, 2004). Although heat from Europa's interior does diffuse through the upper cryosphere, the temperature gradient in the vicinity of a thermal anomaly is essentially unknown because of uncertainties in the thickness of Europa's ice shell, the depth and extent of a convecting ice layer, and the mechanics of cryovolcanism. In any case, due to the relatively small depths of our models (1, 10, and 100 m), the background thermal gradient is unlikely to be a significant thermal component. The only model that has a thermal gradient is the chaos model, which has an initial 10 km layer of liquid water or warm ice.

The models consist of horizontal slabs, whose number and resolution varies depending on the model (Table 1). For every slab, net heat gain or loss from/to below and above is calculated using a discretized version of Fourier's law:

$$\frac{\Delta Q}{\Delta t} = -k\frac{\Delta T_1}{\Delta z} - k\frac{\Delta T_2}{\Delta z}, \tag{1}$$

where Q is heat per unit area. The unit area is assigned a value of 1 in this one-dimensional model for simplicity. ΔT_1 is the temperature difference between the current slab and the slab above, ΔT_2 is the temperature difference between the current slab and the slab below, Δt is the timestep, Δz is slab thickness, and k is thermal conductivity. The new temperature of a slab is then be calculated by

$$T_{\text{new}} = T_{\text{old}} + \frac{\Delta Q}{\rho c_{\text{p}} \Delta z}, \tag{2}$$

where ρ is the density of ice (0.92 g/cm^3), and c_{p} is heat capacity.

All models start with a very thin (<1% the thickness of the water layer) layer of 250 K ice overlying either a body of water at the maximum-density temperature of 276.98 K (Melosh et al., 2004) or a slab of 272 K ice. This temperature was chosen as a reasonable approximation for a variety of resurfacing features; for example, Miyamoto et al. (2005) conclude that temperatures >260 K are needed for formation of ice flow features on Europa, and simulations by Showman and Han (2005) of chaos formation show near-surface convecting ice plumes above 260 K. Depending on the temperature, the model material is assumed to be pure liquid water or ice 1 h, which is consistent with the phase diagram of water under the conditions in Europa's crust. The thermal conductivity and heat capacity of ice in the model vary as a function of temperature, as described by Slack (1980) and Murphy and Koop (2005), respectively.

The temperature of the upper boundary of the model represents a balance between conductive heat flux from below, thermal radiation to space, absorbed sunlight, and sublimation cooling, which is described by the equation

$$\kappa\left(\frac{\partial T(z,t)}{\partial z}\right)_{z=0} = \varepsilon\sigma T^4(0,t) - (1-A)F_{\text{S}}(t) + Lp_{\text{v}}\sqrt{\frac{m}{2\pi RT}}, \tag{3}$$

where κ is thermal conductivity, ε is emissivity, σ is the Stefan–Boltzmann constant, A is the bolometric albedo, L is the latent heat of sublimation, p_{v} is the vapor pressure of ice, m is the molecular weight of H_2O, R is the universal gas constant, and F_{S} is the time-dependent flux of incident sunlight, which cycles as Europa completes a rotation every 3.5512 Earth days. Bolometric albedo and emissivity are set to typical Europa values of 0.55 and 0.9, respectively (Spencer et al., 1999). The bottom boundary is placed sufficiently far away from the surface to avoid boundary effects, and is set to a constant temperature. This "deep temperature" is calculated by running the model without a water or warm ice layer, with insolation as the only heat source. In the chaos (10 km) model, the bottom boundary is set to a constant temperature of 276.98 K to represent the ocean contact. This temperature was chosen following Melosh et al. (2004), who conclude that most of the ocean is at the temperature of maximum density, and that some melt-through events can be explained by the contact between the warm water at maximum density and the ice shell. The possible presence of salts and ammonia in the ocean may reduce the temperature of maximum density of the water by up to a few K for plausible compositions (e.g., Kargel, 1991); however, in this model we neglect this effect and start with the water temperature at 276.98 K.

The thermal inertia Γ of a planetary surface is defined as

$$\Gamma = \sqrt{\kappa\rho c}, \tag{4}$$

where κ is thermal conductivity, ρ is density, and c is the specific heat capacity. Voyager and Galileo observations of Europa (e.g., Spencer et al., 1999) found that the thermal inertia of the surface is $\sim 7 \times 10^4$ erg cm^{-2} s^{-1} K$^{-1/2}$, or ~30 times lower than that of solid water ice (Hansen, 1972), implying a highly unconsolidated surface. An unconsolidated surface above a thermal anomaly, with thermal inertia in this range, is a plausible consequence of the turbulent disruption of the ice/water mixture during freezing as a result of nucleation and growth of vapor bubbles (e.g., Cassen et al., 1979). To evaluate the possible effects of this phenomenon, a 7.5-cm insulating layer with $\Gamma = 7 \times 10^4$ erg cm^{-2} s^{-1} K$^{-1/2}$ is included at the upper boundary of some models. An end-member scenario is assumed, in which the lower thermal inertia is due solely to lower thermal conductivity ($\kappa = 2.52 \times 10^2$ erg g^{-1} cm^{-1} K^{-1} at 273 K).

We conservatively adopt a temperature of 5 K above ambient as the detection limit for a cooling thermal anomaly. While smaller temperature differences are probably detectable from Europa orbit, identification of an endogenic anomaly requires correction for albedo and thermal inertia effects, which may be difficult to do with a precision better than 5 K.

3. Results

For all simulations, except those with an insulating layer, the modeled surface temperature drops almost immediately to ~200 K due to a rapid heat loss by sublimation. For models with an insulating layer, temperature drops even more rapidly to below ~150 K. Following this rapid drop, temperatures decline more gradually, with the rate of cooling roughly proportional to the difference between the surface temperature and the equilibrium temperature due to solar heating.

3.1. 1-m water/warm ice layer

Our simulations indicate that a 1-m layer of water emplaced onto the surface of Europa would freeze completely in ~4 Earth days if the effects of evaporation and sublimation mass loss are neglected. In reality, the crystallization timescale would be even shorter, as a significant fraction of the water would likely boil away before a coherent ice carapace is established (e.g., Cassen et al., 1979). Also, ~10 cm (10% of the slab) would be lost due to sublimation. This thermal anomaly would cease to be

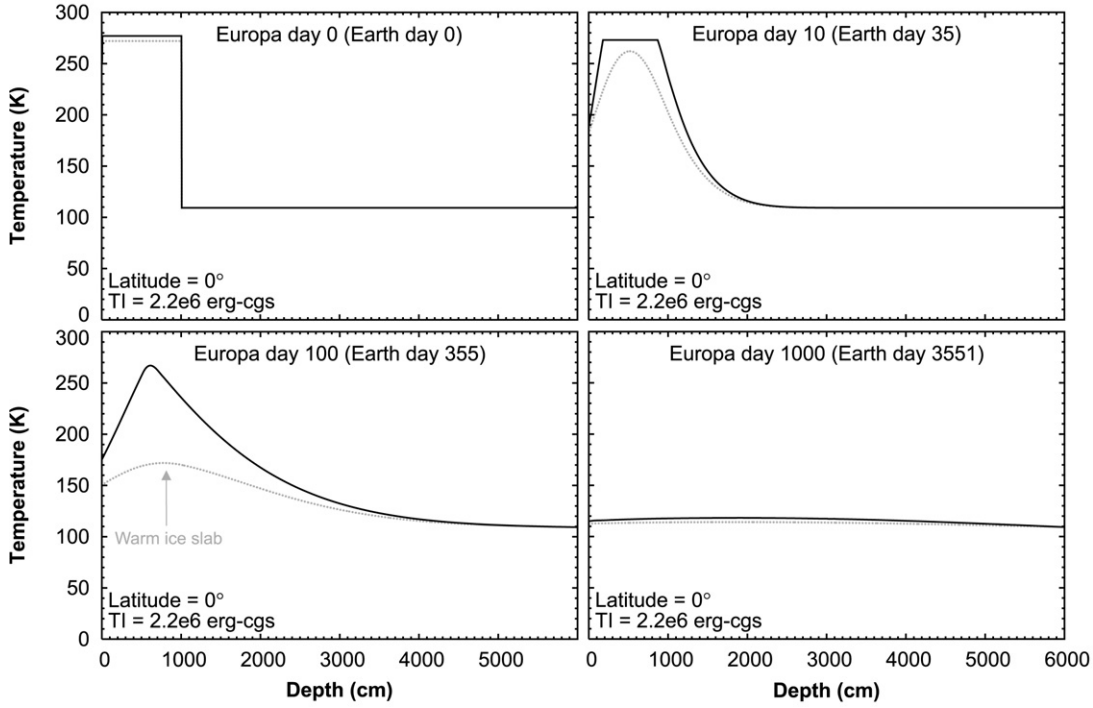

Fig. 3. Subsurface temperature profiles showing the cooling of a 10-m slab of liquid water on the surface of Europa. Temperature profiles for a cooling 10-m slab of warm (272 K) ice are also shown for comparison. An initial 7.5 cm overlying layer of warm (250 K) ice is present in both cases. The thermal inertia (TI) is 2.2×10^6 erg cm^{-2} s$^{-1/2}$ K^{-1}, consistent with low-porosity water ice.

Table 1
Model parameters

Grid	6008 horizontal slabs (models with an insulating layer) 1202 horizontal slabs (all other models except chaos) 1002 horizontal slabs (chaos model)
Spatial resolution	1 cm/slab (models with an insulating layer) 0.5 cm/slab (1-m water/warm ice layer model) 5 cm/slab (10-m water/warm ice layer model) 50 cm/slab (100-m water/warm ice layer model) 1000 cm/slab (10,000-m chaos model)
Temporal resolution	5 s (models with an insulating layer) 0.7 s (1-m water/warm ice layer model) 60 s (10-m water/warm ice layer model) 1500 s (100-m water/warm ice layer model, 10,000-m chaos model)
Heat capacity	$f(T)$, 2.11×10^7 erg/(g K) at 273 K
Density	0.92 g/cm^3
Thermal conductivity	$f(T)$, 2.49×10^5 erg/(g cm K) at 273 K $f(T)$, 2.52×10^2 erg/(g cm K) at 273 K, for the insulating layer
Albedo	0.55
Emissivity	0.9

detectable after 0.27 Earth years (Fig. 8) at equatorial latitudes. If the model is run with an initial 272 K ice layer instead of a 276.98 K water layer, the anomaly would cease to be detectable slightly earlier, at 0.23 Earth years.

3.2. 10-m water/warm ice layer

Subsurface and surface temperatures during the cooling of a 10-m layer of water and a 10-m layer of ice are shown in Figs. 3 and 4. The water layer is maintained at a roughly constant temperature just above freezing by convection, until it is fully crystallized after ∼1 Earth year. Throughout cooling, ∼50 cm (5% of the slab) would be lost due to sublimation. Cooling continues until the thermal anomaly is no longer detectable after 11 Earth years. In case of a warm ice layer, the anomaly would cease to be detectable after 8 Earth years.

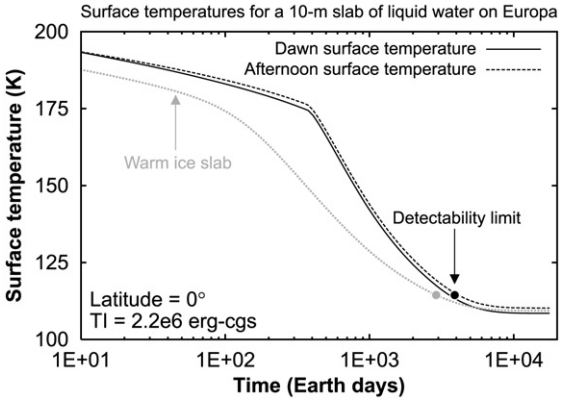

Fig. 4. Surface temperature of ice above a cooling 10-m slab of liquid water. The initial thickness of the overlying ice is 7.5 cm. The kink in the surface temperature occurs when the last liquid water freezes. A cooling curve for a 10-m slab of warm (272 K) ice is also shown for comparison. The thermal inertia (TI) is 2.2×10^6 erg cm^{-2} s$^{-1/2}$ K^{-1}, consistent with low-porosity water ice.

3.2.1. Effects of an insulating upper layer

We also modeled the effects of a 7.5-cm insulating surface layer, as described in Section 2. Comparing Fig. 5 with Fig. 4, note that the presence of an insulating upper layer results in

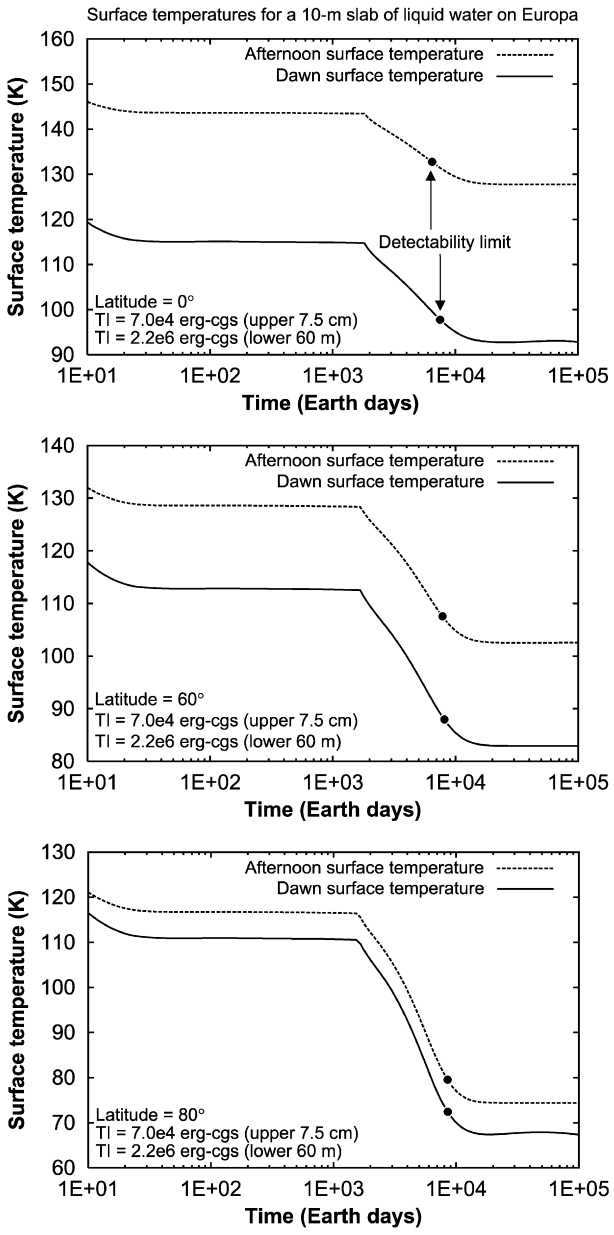

Fig. 5. Surface temperature of insulating ice above a cooling 10-m slab of liquid water at latitudes of 0°, 60° (upper right), and 80° (lower right). The overlying 7.5 cm ice layer has a much lower thermal inertia (TI) than the rest of the model.

much more pronounced diurnal temperature variations, as well as the doubling of the thermal anomaly lifetime. Because of the rapid drop of surface temperature to below ∼150 K, essentially no mass would be lost due to sublimation.

3.2.2. *Effects of latitude*

Solar insolation, and, consequently, surface temperatures, decrease with increasing latitude. The net result of this is that, while a high-latitude anomaly cools faster, it takes up to ∼50% longer for a thermal anomaly at a latitude of 80° to cool to the lower ambient temperatures. This generalization holds true whether the model has an upper insulating layer (Fig. 5) or not (not shown). Combined, the effects of an insulating layer and an increase in latitude from the equator to 80° can more than

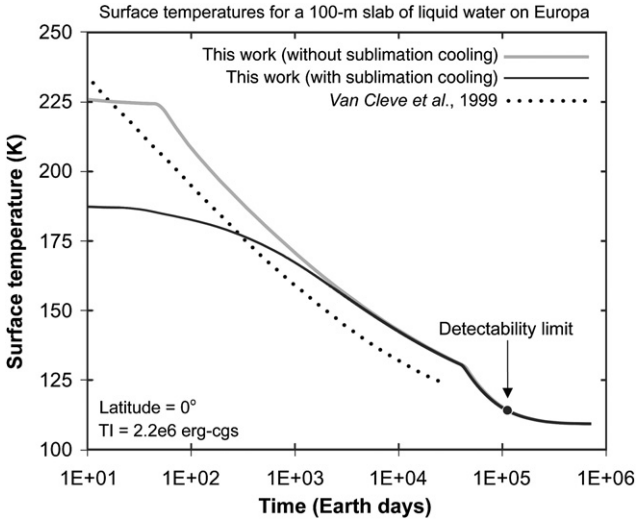

Fig. 6. Diurnal-average surface temperature of ice above a cooling 100-m slab of liquid water (solid lines) compared to a similar model of Van Cleve et al. (1999) (dotted line). The numerical model without sublimation cooling (gray line) is shown for a direct comparison. The initial thickness of the overlying ice is 75 cm.

double the detectable lifetime of this type of a thermal anomaly.

3.3. *100-m water/warm ice layer*

A 100-m layer of water (Fig. 6) takes ∼100 years for the water to freeze completely, but the associated thermal anomaly remains detectable for an a total of 290 years. Throughout cooling, ∼100 cm (1% of the slab) would be lost due to sublimation. In the case of an initial warm ice layer, the thermal anomaly would remain detectable for only 150 years.

Fig. 6 also presents a comparison between our numerical model and the analytical approximation by Van Cleve et al. (1999), which has a water layer of infinite depth but is directly comparable to ours while liquid water remains. However, Van Cleve et al. (1999) did not include sublimation cooling, so for the purposes of this comparison a version of our model without sublimation cooling is used. Another difference between our model and that of Van Cleve et al. (1999) is that our model takes ∼60 days for the water to cool down to 273 K, whereas their model starts at 273 K. Subsequently, the Van Cleve et al. (1999) model consistently underestimates the surface temperature by ∼10 K compared to our model. If both models start at the freezing point of water (not shown), the analytical solution initially overestimates temperatures, but after ∼50 days crosses the numerical curve and underestimates temperatures by ∼10 K. The discrepancy may result from approximations in the analytical model: a similar discrepancy between full numerical models and a similar analytical approximation was noted in cooling models for Io lava flows by Howell (1997).

3.3.1. *Effects of latitude*

The 100-m water layer model was also run at latitudes of 60° and 80°, and our results indicate that the detectable lifetime would be 40 to 90% longer, respectively. Note that in the

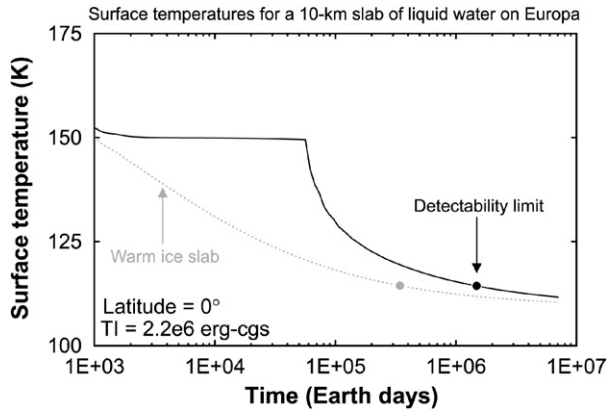

Fig. 7. Diurnal-average surface temperature of ice above a cooling 10-km slab of liquid water (solid line) or warm (272 K) ice (dashed line). The bottom boundary of this model is held at a constant 276.98 K. The initial thickness of the overlying ice is 15 m.

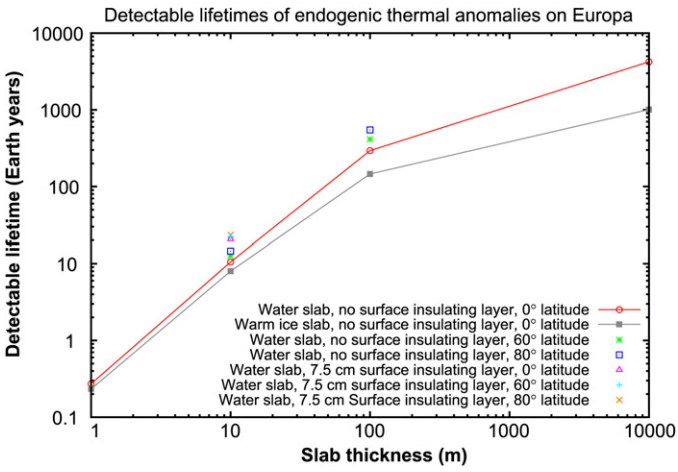

Fig. 8. Lifetimes of modeled thermal anomalies (the duration for which they would remain detectable by a thermal mapping instrument on a future mission).

100-m model, the detectable lifetime has a stronger dependence on latitude than the 10-m model, because water takes a proportionally longer time to freeze completely and therefore the anomaly remains a proportionally longer time above the background temperature. It is likely that the latitude dependence will be even stronger for deeper models as suggested by Van Cleve et al. (1999).

3.4. 10-km chaos model

The thermal evolution of a freshly-formed chaos region is shown in Fig. 7. A melt-through type of chaos was modeled with a 10-km layer of water overlain by an initial 15-m layer of 250 K ice. Note that the chaos model is different from the previous models in that it includes a warm lower boundary and this a steady supply of endogenic heat. For simplicity, it was assumed that the temperature of the water in the model would remain homogeneous during cooling, due to convection/overturn processes. Thus, freezing does not begin until the water reaches 273.15 K in 160 Earth years (this is represented by a kink in Fig. 7). In reality, a cold boundary layer likely would have formed at the top of the water layer, resulting in an earlier start of crystallization. Nonetheless, the time span before the onset of freezing is small compared to the time the thermal anomaly remains detectable, which is 4200 Earth years. This also illustrates that the lifetime of this thermal anomaly is not strongly dependent on the temperature of the ocean, as starting at 273.15 K would result in the shortening of the detectable lifetime by 160 years (~4%) at most.

Another possible chaos formation mechanism is ice mobilization by convection, diapirism, or similar processes. This was modeled with a 10-km layer of 272 K ice overlain by an initial 15-m layer of 250 K ice. Our simulations indicate that the thermal anomaly associated with this type of chaos would remain detectable for 1000 years.

3.5. Number of detectable thermal anomalies

The number of detectable thermal anomalies N on Europa at any given time can be expressed as

$$N = \frac{At}{2Ta}, \tag{5}$$

where T is the average surface age of Europa (~60 Ma), A is its surface area (3.06×10^7 km^2), t is the detectable lifetime of a thermal anomaly produced by a resurfacing event, and a is the typical area resurfaced by a single event. If a typical size of a resurfacing event is ~15 km^2, as suggested by some Galileo imagery (e.g., the "pond" in Fig. 1, and a flat, smooth area in NASA press release image PIA00592) then $N = 0.02t$, where t is in years. On the other hand, if recent resurfacing on Europa has been dominated by chaos formation, as suggested by Pappalardo et al. (1999) and Figueredo and Greeley (2004), and the typical chaos area is ~100 km^2 (Greenberg et al., 1999, Fig. 7), then $N = 0.003t$.

The results of this study, summarized in Fig. 8, suggest that, if a typical thickness of a liquid water eruption is 100 m and area is 15 km^2, at least 6 such events should be detectable. If the typical thickness is 10 m, the number of detectable events drops to 0.5 or lower, depending on latitude and surface properties. If warm ice instead of liquid water is emplaced, the anomaly cools faster and the number of detectable events further decreases by up to 50%, depending on the thickness of the anomaly. On the other hand, if chaos formation is the primary mode of resurfacing, the number of detectable events is at least 13 for melt-through chaos, and 3 for ice mobilization chaos. These estimates assume that (i) resurfacing events occur at regular intervals, (ii) most resurfacing events involve liquid water or warm ice at or near the surface, and (iii) each resurfacing event is independent. The last assumption may be problematic in the case of chaos formation, as a single melt-through or convection event may form multiple chaos regions. For example, if ten typical-sized chaos regions are created per event, for a combined area of 1000 km^2, the number of detectable thermal anomalies would drop to 0.3 to 1.3, depending on chaos formation mode.

4. Conclusions

The results of this numerical study suggest that the detectable lifetime of a thermal anomaly associated with the em-

placement of 100 m of water onto the surface of Europa is several hundred years, which is consistent with an analytical calculation performed by Van Cleve et al. (1999). For a thermal anomaly associated with a 10-m layer of water, the expected lifetime is on the order of 10 years. If warm ice is emplaced on the surface instead of liquid water, the above lifetimes decrease by up to 50%. The results also indicate that the presence of a thin insulating surface layer can extend thermal anomaly lifetimes by up to a factor of two, that thermal anomalies emplaced at a latitude of 80° remain detectable for up to 90% longer than anomalies at equatorial latitudes, and that thermal anomalies remain detectable for up to ∼20% longer on the night side compared to the day side. Thus, a thermal infrared survey of high latitudes at the night side is more likely to yield positive results. However, a comparison of day and night temperatures will be required to distinguish endogenic anomalies (which will be anomalously warm at all times of the day) from high thermal inertia regions (which will be warm at night but cool during the day). A detection of high thermal inertia regions would also be interesting in its own right, because these regions may in themselves be sites of recent activity if the high thermal inertia is due to the lack of a mature regolith on a young surface.

Based on the results of this study, the number of detectable thermal anomalies associated with the emplacement of 100 m of water would be on the order of 10 if the typical resurfacing area is 15 km^2; for 10 m of water, that number is between 0.2 and 0.5. For surface emplacement of warm ice, the number of detectable events decreases by up to a factor of two. These numbers are inversely proportional to the area of a typical resurfacing event, which is poorly constrained. For example, recent resurfacing may be dominated by chaos formation, which remains detectable for 1000 to 4200 years depending on whether it is formed by liquid water melt-through or ice mobilization. If this is the case, and a typical chaos event has an area of 100 km^2, 3 to 13 thermal anomalies would be detectable, depending on chaos mode of formation. If a typical chaos event covers an area of 1000 km^2, the number of detectable anomalies drops to 0.3 to 1.3. So while the size and thickness of recent resurfacing events on Europa is quite uncertain, plausible values for these parameters, when combined with the anomaly lifetimes determined from this work, suggest that several detectable endogenic thermal anomalies could plausibly exist. Thermal infrared mapping is therefore a potentially powerful tool in the search for recent geological activity on Europa.

Acknowledgments

This work was supported by Southwest Research Institute internal research grant R9598 and NASA Outer Planets Research grant NNG06GF41G. We thank Jeffrey Van Cleve and an anonymous reviewer for thorough and constructive reviews of this manuscript.

References

Carr, M.H., Belton, M.J.S., Chapman, C.R., Davies, M.E., Geissler, P., Greenberg, R., McEwen, A.S., Tufts, B.R., Greeley, R., Sullivan, R., Head, J.W., Pappalardo, R.T., Klaasen, K.P., Johnson, T.V., Kaufman, J., Senske, D., Moore, J., Neukum, G., Schubert, G., Burns, J.A., Thomas, P., Veverka, J., 1998. Evidence for a subsurface ocean on Europa. Nature 391, 363–365.

Cassen, P.M., Reynolds, R.T., Peale, S.J., 1979. Is there liquid water on Europa? Geophys. Res. Lett. 6, 731–734.

Fagents, S.A., Kadel, S.D., Greeley, R., Kirk, R.L., and the Galileo SSI team, 1998. Styles of cryovolcanism on Europa: Summary of evidence from the Galileo nominal mission. Lunar Planet. Sci. XXIX. Abstract 1721.

Figueredo, P.H., Greeley, R., 2004. Resurfacing history of Europa from pole-to-pole geological mapping. Icarus 167, 287–312.

Greenberg, R., Geissler, P., Hoppa, G., Tufts, B.R., Durda, D.D., 1998. Tectonic processes on Europa: Tidal stresses, mechanical response, and visible features. Icarus 135, 64–78.

Greenberg, R., Hoppa, G.V., Tufts, B.R., Geissler, P., Riley, J., 1999. Chaos on Europa. Icarus 141, 263–286.

Hansen, O.L., 1972. Thermal radiation from the Galilean satellites measured at 10 and 20 microns. Ph.D. thesis, California Institute of Technology, Pasadena.

Head, J.W., Pappalardo, R.T., Greeley, R., Sullivan, R.J., and the Galileo Imaging Team, 1998. Origin of ridges and bands on Europa: Morphologic characteristics and evidence for linear diapirism from Galileo data. Lunar Planet. Sci. XXIX. Abstract 1414.

Head III, J.W., Pappalardo, R.T., 1999. Brine mobilization during lithospheric heating on Europa: Implications for formation of chaos terrain, lenticula texture, and color variations. J. Geophys. Res. 104, 27143–27156.

Hoppa, G.V., Tufts, B.R., Greenberg, R., Geissler, P.E., 1999. Formation of cycloidal features on Europa. Science 285, 1899–1902.

Howell, R.R., 1997. Thermal emission from lava flows on Io. Icarus 127, 394–407.

Hussmann, H., Spohn, T., 2004. Thermal-orbital evolution of Europa. Icarus 171, 391–410.

Kadel, S.D., Fagents, S.A., Greeley, R., and the Galileo SSI team, 1998. Trough-bounding ridge pairs on Europa-considerations for an endogenic model of formation. Lunar Planet. Sci. XXIX. Abstract 1078.

Kargel, J.S., 1991. Brine volcanism and the interior structures of asteroids and icy satellites. Icarus 94, 368–390.

Ketkar, S.P., 1999. Numerical Thermal Analysis. American Society of Mechanical Engineers, New York.

Khurana, K.K., Kivelson, M.G., Stevenson, D.J., Schubert, G., Russell, C.T., Walker, R.J., Joy, S., Polanskey, C., 1998. Induced magnetic fields as evidence for subsurface oceans in Europa and Callisto. Nature 395, 777–780.

Kivelson, M.G., Khurana, K.K., Russell, C.T., Volwerk, M., Walker, R.J., Zimmer, C., 2000. Galileo magnetometer measurements: A stronger case for a subsurface ocean at Europa. Science 289, 1340–1343.

McKinnon, W.B., 1999. Convective instability in Europa's floating ice shell. Geophys. Res. Lett. 26, 951–954.

Melosh, H.J., Turtle, E.P., 2004. Ridges on Europa: Origin by incremental ice-wedging. Lunar Planet. Sci. XXXV. Abstract 2029.

Melosh, H.J., Ekholm, A.G., Showman, A.P., Lorenz, R.D., 2004. The temperature of Europa's subsurface water ocean. Icarus 168, 498–502.

Miyamoto, H., Mitri, G., Showman, A.P., Dohm, J.M., 2005. Putative ice flows on Europa: Geometric patterns and relation to topography collectively constrain material properties and effusion rates. Icarus 177, 413–424.

Murphy, D.M., Koop, T., 2005. Review of the vapor pressures of ice and supercooled water for atmospheric applications. Q. J. R. Meteorol. Soc. 131, 1539–1565.

O'Brien, D.P., Geissler, P., Greenberg, R., 2002. A melt-through model for chaos formation on Europa. Icarus 156, 152–161.

Ojakangas, G.W., Stevenson, D.J., 1989. Thermal state of an ice shell on Europa. Icarus 81, 220–241.

Pappalardo, R.T., Head, J.W., Greeley, R., Sullivan, R.J., Pilcher, C., Schubert, G., Moore, W.B., Carr, M.H., Moore, J.M., Belton, M.J.S., Goldsby, D.L., 1998. Geological evidence for solid-state convection in Europa's ice shell. Nature 391, 365–368.

Pappalardo, R.T., Belton, M.J.S., Breneman, H.H., Carr, M.H., Chapman, C.R., Collins, G.C., Denk, T., Fagents, S., Geissler, P.E., Giese, B., Greeley, R.,

Greenberg, R., Head, J.W., Helfenstein, P., Hoppa, G., Kadel, S.D., Klaasen, K.P., Klemaszewski, J.E., Magee, K., McEwen, A.S., Moore, J.M., Moore, W.B., Neukum, G., Phillips, C.B., Prockter, L.M., Schubert, G., Senske, D.A., Sullivan, R.J., Tufts, B.R., Turtle, E.P., Wagner, R., Williams, K.K., 1999. Does Europa have a subsurface ocean? Evaluation of the geological evidence. J. Geophys. Res. 104 (E10), 24015–24055.

Schenk, P.M., Chapman, C.R., Zahnle, K., Moore, J.M., 2004. Ages and interiors: The cratering record of the Galilean satellites. In: Bagenal, F., Dowling, T.E., McKinnon, W.B. (Eds.), Jupiter: The Planet, Satellites and Magnetosphere. Cambridge Univ. Press, Cambridge, pp. 427–456.

Showman, A.P., Han, L., 2005. Effects of plasticity on convection in an ice shell: Implications for Europa. Icarus 177, 425–437.

Slack, G.A., 1980. Thermal conductivity of ice. Phys. Rev. B 22 (6), 3065–3071.

Sotin, C., Tobie, G., 2004. Internal structure and dynamics of the large icy satellites. C. R. Acad. Sci. Phys. 5, 769–780.

Sotin, C., Head, J.W., Tobie, G., 2002. Europa: Tidal heating of upwelling thermal plumes and the origin of lenticulae and chaos melting. Geophys. Res. Lett. 29 (8), doi:10.1029/2001GL013844. 1233.

Spencer, J.R., Tamppari, L.K., Martin, T.Z., Travis, L.D., 1999. Temperatures on Europa from Galileo PPR: Nighttime thermal anomalies. Science 284, 1514–1516.

Sullivan, R., Greeley, R., Klemaszewski, J., Kraft, M., Moreau, J., Williams, K., Belton, M., Carr, M., Chapman, C., Clark, B.E., Geissler, P., Greenberg, R., Tufts, B.R., Head, J., Pappalardo, R., Moore, J.M., 1997. Ridge formation on Europa: Examples from Galileo high resolution images. Geol. Soc. Am. Abstr. Programs 29. A-312.

Van Cleve, J.E., Pappalardo, R.T., Spencer, J.R., 1999. Thermal palimpsests on Europa: How to detect sites of current activity. Lunar Planet. Sci. XXX. Abstract 1815.

Zahnle, K., Dones, L., Levison, H.F., 1998. Cratering rates on the Galilean satellites. Icarus 136, 202–222.